NASA Technical Memorandum 102402
ICOMP-89-29

Two-Dimensional Euler and Navier Stokes Time Accurate Simulations of Fan Rotor Flows

A.A. Boretti
Centro Ricerche FIAT—MOTORI
Orbassano, Italy

and Institute for Computational Mechanics in Propulsion
Lewis Research Center
Cleveland, Ohio

July 1990

NASA

INSTITUTE FOR COMPUTATIONAL MECHANICS IN PROPULSION
NASA LEWIS RESEARCH CENTER
ICOMP
CASE WESTERN RESERVE UNIVERSITY

TWO-DIMENSIONAL EULER AND NAVIER STOKES TIME ACCURATE SIMULATIONS OF FAN ROTOR FLOWS

A.A. Boretti

Centro Ricerche FIAT - MOTORI
Orbassano, Italy

and

Institute for Computational Mechanics in Propulsion*
Lewis Research Center
Cleveland, Ohio

SUMMARY

This report presents two numerical methods to describe the unsteady flow field in the blade-to-blade plane of an axial fan rotor. These methods solve the compressible, time-dependent, Euler and the compressible, turbulent, time-dependent, Navier-Stokes conservation equations for mass, momentum, and energy. The Navier-Stokes equations are written in Favre-averaged form and are closed with an approximate two-equation turbulence model with low Reynolds number and compressibility effects included. The unsteady aerodynamic component is obtained by superposing inflow or outflow unsteadiness to the steady conditions through time-dependent boundary conditions. The integration in space is performed by using a finite-volume scheme, and the integration in time is performed by using k-stage Runge-Kutta schemes, k = 2,5. The numerical integration algorithm allows the reduction of the computational cost of an unsteady simulation involving high-frequency disturbances in both CPU time and memory requirements. Less than 200 sec of CPU time are required to advance the Euler equations in a computational grid made up of about 2000 grid points during 10 000 time steps on a CRAY Y-MP computer, with a required memory of less than 0.3 megawords.

INTRODUCTION

The reduction of automotive fan noise is now the subject of vigorous research. A better understanding of fan noise generation calls for a proper description of the physical processes which connect unsteady flow interactions with fan blades to far field noise. The unsteady aerodynamic component of the fan flow field is linked to the resultant far field acoustic pattern via the blade unsteady aerodynamic response, the coupling with the duct, the propagation in the duct, and the acoustic coupling to the far field noise. The present work is devoted to numerically simulating the unsteady flow field through the blades of an axial flow fan rotor by solving the Euler and Navier-Stokes equations.

---

*Work funded by Space Act Agreement C-99066-G.

In a classical description of the fan flow field, the actual three-dimensional flow is built up by superposing two two-dimensional flow solutions to yield a quasi-three-dimensional flow field. The first solution is a through-flow solution, which treats the circumferentially averaged flow. The through-flow solution defines the flow conditions upstream and downstream of the rotor blades on axisymmetric surfaces. The second solution is a blade-to-blade flow solution on these surfaces, defining the flow conditions inside the rotor blade passage.

In a design approach, simplified through-flow and blade-to-blade solutions plus empirical correlations are used to define the shape of the airfoils along the blade-to-blade surfaces. These airfoils are then staked to generate the blade. The staking includes blade forward skew resulting from simplified acoustic solutions for the isolated airfoil unsteady aerodynamic response plus simplified solutions for the acoustic coupling to the far field. The resulting fan geometries are therefore tested experimentally in order to assess the overall performances.

In an improved design approach, analytical methods become useful to introduce changes in blade shape. These changes are usually defined by using steady flow analysis methods in order to improve steady blade performances. The use of unsteady flow analysis methods should be able to improve both steady and unsteady blade performances. The present report describes two computer codes developed to study the steady and unsteady flow on the blade-to-blade surfaces. The flow field is predicted by numerically solving the compressible, time-dependent, Euler and the compressible, turbulent, time-dependent, Navier-Stokes conservation equations for mass, momentum, and energy. The areas of major concern in solving the governing conservation equations are the modeling of turbulence in the Navier-Stokes conservation equations, the formulation and implementation of appropriate boundary conditions, and the formulation of a time-accurate numerical integration algorithm.

The Navier-Stokes equations are written in Favre-averaged form. The conservation equations for mass, momentum, and energy are closed by using a two-equation turbulence model with low Reynolds number and compressibility effects included. The turbulence model is valid only for steady flows, but despite the lack of theory, the prediction capability of two-equation turbulence models in unsteady flow computations is not worse than the one obtained in steady flow computations. The proposed turbulence model suggests wall and compressibility corrections to standard K-ε turbulence models in order to extend their range of applicability to compressible and separated flow fields. Apart from the values of the model constants actually specified, the model should be able to properly predict the flow turbulence when experimental data are available in enough detail to guide the model development and fix the values of the constants better.

The unsteady aerodynamic response is obtained by superposing inflow or outflow unsteadiness to the steady conditions. For an unexcited jet flow, the inflow total pressure and density and the outflow static pressure are specified at constant values. To facilitate investigating the influence of acoustic or pressure excitation, the inflow total pressure and total density or the outflow static pressure are modified by imposing time-dependent values. The time dependence is usually accomplished by imposing a sinusoidal oscillation to the steady values or a simpler step function. For now, the unsteady blade

performances can be defined in terms of blade pressure fluctuation amplitude normalized by the forcing pressure perturbation amplitude, but further work is needed in order to better define these unsteady blade performances.

The integration in space is performed by using a finite-volume scheme. Along the boundaries, all of the flow parameters not specified by a boundary condition are computed by solving their conservation equations over half of the control volumes. The integration in time is performed by using multistage Runge-Kutta schemes. The numerical integration algorithm has been developed with the aim of reducing the computational cost of an unsteady simulation involving high-frequency disturbances. The finite-volume formulation is adopted to allow the use of an arbitrary grid in the application to complex flow geometries. The multistage Runge-Kutta scheme is used both to improve accuracy in time and to extend the stability region of the explicit discretization. Two-, three-, four-, or five-stage Runge-Kutta schemes similar to Jameson's (Jameson et al., 1981) are used. A k-stage scheme can be made stable for a Courant number up to k - 1, but these schemes cannot be more than second-order accurate in time (Chima, Turkel, and Schaffer, 1987). The order of the scheme can be selected in accordance with the stability requirements for the particular problem. Dissipative terms have been added to suppress the tendency for odd and even points decoupling and to prevent the appearance of wiggles in regions containing severe pressure gradients. The numerical dissipation is introduced as the difference between second- and fourth-order differences. The magnitude of the dissipative terms has been adapted to the local flow properties by means of a sensor based on the local pressure gradient. The overall accuracy is second order in both space and time.

EULER EQUATIONS

The computation of high Reynolds number, unseparated, unsteady cascade flow fields can be easily accomplished by solving the Euler conservation equations written in unsteady, compressible form. The basic variables are the gas density, velocity, and enthalpy. Their conservation equations are written as follows:

$$\rho_{,t} + (\rho u_k)_{,k} = 0$$

$$(\rho u_i)_{,t} + (\rho u_k u_i)_{,k} = -p_{,i}$$

$$(\rho h_0)_{,t} + (\rho u_j h_0)_{,j} = p_{,t}$$

where the state equation is

$$p = (\gamma - 1)/\gamma \cdot \rho \cdot h$$

The integration of the previous equations requires the introduction of the conditions to be fulfilled along the boundaries of the domain of interest. The physical flow domain is represented in figure 1. (As an aid to the reader, a symbols list has been included in the appendix.) The flow domain is limited by inflow, outflow, solid, and periodic boundaries, where appropriate boundary conditions are needed. Along the inflow boundary, the total pressure p_{01}, total density ρ_{01}, and flow angle β_1 are specified, whereas the Mach number is extrapolated from the interior. These values can be both steady or time dependent. Along the outflow boundary, the static pressure p_2 is specified,

whereas all other variables are extrapolated from the interior. The value used for the static pressure can be steady or time dependent. The inflow and outflow boundary-condition values are assumed to be constant in the pitchwise direction, as theoretically fulfilled only at the upstream and downstream infinite. Across the solid boundaries, the flux of mass and energy is set equal to zero, whereas the flux of momentum is evaluated from the blade pressure and all of the variables are extrapolated from the interior.

Before starting the time integration, proper initial conditions have to be specified. These conditions can be either a previously computed steady-state condition or a simple no-flow condition.

NAVIER-STOKES EQUATIONS

A better description of the unsteady flow field can be accomplished by solving the Navier-Stokes conservation equations. The solution of the Navier-Stokes equations is required in the study of the cascade flow field at off-design conditions, when the incidence effects play an important role. The full Navier-Stokes conservation equations are written in unsteady, compressible form. The basic variables are the gas density, velocity, and enthalpy. Their conservation equations are written in Favre-averaged form as follows:

$$\bar{\rho}_{,t} + (\bar{\rho}\,\tilde{u}_k)_{,k} = 0$$

$$(\bar{\rho}\,\tilde{u}_i)_{,t} + (\bar{\rho}\,\tilde{u}_k\,\tilde{u}_i)_{,k} = -\bar{p}_{,i} + \left(\bar{\tau}_{ik} - \overline{\rho\,u''_k\,u''_i}\right)_{,k}$$

$$(\bar{\rho}\,\tilde{\tilde{h}}_0)_{,t} + (\bar{\rho}\,\tilde{u}_j\,\tilde{\tilde{h}}_0)_{,j} = \bar{p}_{,t} + \overline{u''_j\,p_{,j}} + [-\bar{q}_j - \overline{\rho\,u''_j\,h''}]_{,j}$$

$$+ [\bar{\tau}_{ij}\,\tilde{u}_i - \overline{\rho\,u''_i\,u''_j}\,\tilde{u}_i]_{,j} + \overline{u''_{i,j}\,\tau_{ij}} + \overline{\rho\,u''_i\,u''_k}\,\tilde{u}_{i,k}$$

where (Hirsch and Deconinck, 1985)

$$\tilde{\tilde{h}}_0 = \tilde{h} + \frac{\tilde{u}_i\,\tilde{u}_i}{2} = \tilde{h}_0 - \frac{\overline{\rho\,u_i''\,u_i''}}{2\bar{\rho}}$$

and the state equation is

$$\bar{p} = (\gamma - 1)/\gamma \cdot \bar{\rho} \cdot \tilde{h}$$

and the constitutive relations are

$$\bar{\tau}_{ij} = \mu\left(\tilde{u}_{i,j} + \tilde{u}_{j,i} - \frac{2}{3}\,\tilde{u}_{k,k}\,d_{ij}\right)$$

and

$$q_j = \frac{-\kappa\, h_{,j}}{Pr}$$

The previous equations are not closed, and some empirical expressions have to be introduced for the turbulent quantities. A turbulence model which reflects the availability of experimental data is needed. The closure is achieved by using a first-order turbulence model. These models are probably the most reliable turbulence models because of the availability of experimental results and computer resources. The K-ε turbulence model adopted here includes low Reynolds number terms (to account for near wall effects and to compute separated flows, in accordance with the suggestions given by Boretti and Martelli, 1989a) and includes a pressure-density gradient term (to account for compressibility, in accordance with the suggestions of Jones and McGuirk, 1987). Note that the model is strictly valid only for steady flows but that it can be used in unsteady flow computations without introducing great errors.

The Reynolds stresses and the turbulent heat flux vector are expressed as follows:

$$\overline{\rho\, u''_i\, u''_j} = -\mu_t\left(\tilde{u}_{i,j} + \tilde{u}_{j,i} - \frac{2}{3}\, d_{ij}\, \tilde{u}_{l,l}\right) + \frac{2}{3}\, d_{ij}\, K\, \bar{\rho}$$

$$\overline{\rho\, u''_k\, h''} = \frac{-\mu_t\, \tilde{h}_{,i}}{Pr_t}$$

where

$$\mu_t = \frac{\bar{\rho}\, C_\mu\, f_\mu\, K^2}{\varepsilon}$$

The Favre-averaged conservation equations for K and ε are written as follows:

$$(\bar{\rho}\, K)_{,t} + (\bar{\rho}\, \tilde{u}_i\, K)_{,i} = \left[\frac{K_{,i}}{Sc_K(\mu_t + \mu)}\right]_{,i} + P + F - \bar{\rho}\, \varepsilon + D$$

$$(\bar{\rho}\, \varepsilon)_{,t} + (\bar{\rho}\, \tilde{u}_i\, \varepsilon)_{,i} = \left[\frac{\varepsilon_{,i}}{Sc_e(\mu_t + \mu)}\right]_{,i} + \frac{\varepsilon}{K}\left[C_{\varepsilon 1}\, f_1\, (P + G) - C_{\varepsilon 2}\, f_2\, \bar{\rho}\, \varepsilon_1\right] + E$$

where the turbulence kinetic energy production is

$$P = -\overline{\rho\, u''_i\, u''_j}\, \tilde{u}_{i,j}$$

the wall terms D and E are (Boretti and Martelli, 1988)

$$D = -2\mu\left[\left(K\right)^{1/2}{}_{,k}\right]^2$$

$$E = -2\mu\left[\left(\varepsilon\right)^{1/2}{}_{,k}\right]^2$$

and the compressibility terms F and G are (Jones and McGuirk, 1987)

$$F = -\frac{\mu_t}{\bar{\rho}^2\,\bar{\rho}_{,i}\,\bar{p}_{,i}}$$

$$G = -\frac{\mu_t}{\bar{\rho}^2\,\bar{\rho}_{,i}\,\bar{p}_{,i}}$$

The compressibility terms F and G play an important role only for high-speed flows, and they have a negligible influence at low speeds.

The values of the model constants are chosen as follows:

$C_\mu = 0.09$ $\quad C_{\varepsilon 1} = 1.43$ $\quad C_{\varepsilon 2} = 1.92$ $\quad Sc_K = 1.0$ $\quad Sc_\varepsilon = 1.3$

and the low Reynolds number functions are expressed as

$$f_\mu = \exp[-2.5/(1 + R_t/50)]$$

$$f_1 = 1.0$$

and

$$f_2 = 1.0 - 0.33\exp[-R_t{}^2]$$

where the turbulent Reynolds number is

$$R_t = \frac{\bar{\rho}\,K^2}{\mu\,\varepsilon}$$

Finally,

$$\overline{u''_j\,p_{,j}} = -\left(\mu_t/\bar{\rho}^2\right)\cdot\bar{\rho}_{,i}\cdot\bar{p}_{,i}$$

and

$$\overline{u''_{i,j}\,\tau_{ij}} = -\bar{\rho}\,\varepsilon$$

The boundary conditions for the Navier-Stokes equations differ from those adopted for the Euler equations because of the influence of viscosity. Along the inflow boundary, the total pressure p_{01}, total density ρ_{01}, flow angle β_1, inlet turbulence level Tu_1,

$$K = Tu\,V^2$$

and the length scale of the turbulence motions Le_1,

$$\varepsilon = \frac{K^{3/2}}{Le}$$

are specified, whereas the Mach number is extrapolated from the interior. These values can be both steady or time-dependent values. Inflow boundary-condition values constant in the pitchwise direction are theoretically fulfilled only at the upstream infinite, but the influence on the cascade flow is not too strong if enough mesh points are used upstream of the blade cascade. Along the outflow boundary, the static pressure p_2 is specified, but all of the other variables are extrapolated from the interior. The value used for the static pressure can be a steady or a time-dependent value. An outflow boundary-condition value constant in the pitchwise direction is theoretically fulfilled only at the downsteam infinite but has no influence on the cascade flow when enough mesh points are used downstream of the blade cascade. Along the solid boundaries, the velocity, turbulence kinetic energy, and turbulence kinetic energy dissipation rate vanish. For adiabatic flows, the temperature gradient normal to the wall is set equal to zero. Otherwise, the temperature is set equal to the wall value. Across the solid boundaries, the flux of mass is set equal to zero, along with the flux of energy for adiabatic flows. The flux of momentum, the flux of energy for nonadiabatic flows, and the fluxes of the turbulent variables are eventually evaluated from the blade pressure and viscous terms. The density is finally extrapolated from the interior.

NUMERICAL METHOD

The computational domain is shown in figure 2. The grid is obtained by the intersection of pseudostreamlines and pitchwise lines. The equations are discretized in space by using a cell-centered, finite-volume formulation. Figure 3 shows the finite-volume molecules approximating inviscid and viscous terms. The time derivatives and the source terms are evaluated at the cell center grid point. The spatial differences are evaluated as net fluxes across the faces of the cell, computed at the cell faces, and divided by the cell area. The discretization in space of the inviscid terms of the Navier-Stokes equations (i.e., the Euler equations) thus requires the cell center grid point and the 6 surrounding grid points. Since the first-order derivatives appearing in the viscous terms of the Navier-Stokes equations (stress tensor, heat flux, and others) are expressed by using 4 grid points, the discretization in space of the Navier-Stokes equations involves 17 grid points. Global conservation is ensured by evaluating the flux vectors on the faces of the boundary conforming mesh cell. Half-cells are used along the inflow, outflow, and solid boundaries. The first-order derivatives appearing in the viscous terms of the Navier-Stokes equations (stress tensor, heat flux, and others) and the first-order derivatives of the inviscid terms are expressed along the boundaries by using one-sided differences. The scheme is second-order accurate in space on a regular grid.

The equations are integrated in time by using explicit, multistage, dissipative, Runge-Kutta algorithms. When the previous time-dependent equations are rewritten in the following vector form

$$f_{,t} = T(f)$$

the solution at the time $t = (m + 1)dt$ is expressed as a function of quantities evaluated at the times $(m)dt$ according to the following scheme:

$$f^{(0)} = f^m$$

$$f^{(1)} = f^{(0)} - C_1\, dt\, [T_i(f^{(0)}) + T_v(f^{(0)}) + AV^2\, D^2(f^{(0)}) - AV^4\, D^4(f^{(0)})]$$

$$f^{(m)} = f^{(0)} - C_k\, dt\, [T_i(f^{(k-1)}) + T_v(f^{(0)}) + AV^2\, D^2(f^{(0)}) - AV^4\, D^4(f^{(0)})]$$

$$f^{(m+1)} = f^{(m)}$$

where D^2 is a term approximating second-order differences, D^4 is a term approximating fourth-order differences, AV^2 is a viscosity coefficient for second-order differences, where

$$AV^2 = C_{(AV^2)}\, abs(D^2(p))/(2\bar{p})$$

with $\bar{p}$ an averaged pressure, and AV^4 is a viscosity coefficient for fourth-order differences

$$AV^4 = \max(0.0,\ C_{(AV^4)} - AV^2)$$

The second-order dissipative term as well as the averaged pressure is evaluated in every mesh cell by using the 7-grid-points scheme of figure 3. Since the fourth-order terms are expressed as second-order differences of second-order differences, the discretization in space of these terms involves the 19 grid points. The residual vector is split into two parts, an inviscid and a viscous one, for convergence-improving purposes. The artificial viscosity coefficients are chosen as follows for Navier-Stokes solutions:

$$C_{(AV^2)} = 0.27 \qquad C_{(AV^4)} = 0.016$$

whereas slightly larger coefficients are used for Euler solutions.

The time step limit for an explicit scheme is established by the classical Courant-Friedrich-Levy stability limit (CFL) for inviscid flows,

$$dt < dr\, \frac{CFL}{a + V}$$

where dr is a characteristic dimension of the space discretization, a is the speed of sound,

$$a^2 = \gamma \cdot \bar{p}/\bar{\rho}$$

and V is the velocity. The order of the multistage Runge-Kutta scheme is selected in accordance with the time step and stability requirements. By

increasing the order of the multistage Runge-Kutta scheme, the maximum CFL number increases, and a proper selection of the scheme order follows from the prescribed time scale of the unsteady flow. A k-stage scheme used with central differencing is stable for a Courant number of approximately $k - 1$, depending on the choice of C_i, $i = 1,k$. The influence of a CFL greater than unity on the maximum time step is shown in figure 4 for a CFL of about 2. For consistency, $C_k = 1$, whereas for second-order accuracy in time $C_{k-1} = 1/2$. Note that the schemes of this form cannot be more accurate than second-order for any values of C_i, $i = 1,k$ (Chima, Turkel, and Schaffer, 1987). The values of C_i, $i = 1,k$ proposed by Chima et al., 1987 for two-, three-, four-, and five-stage schemes are adopted here, allowing CFL numbers of about 1.00, 1.50, 2.75, and 3.50, respectively. A switch parameter enables the choice of the k value. A CFL smaller than the one permitted by a linear inviscid stability analysis is adopted in the solution of the Navier-Stokes equations. This choice was made because of the full coupling of the K-ε conservation equations with the basic variables conservation equations and the neglected viscous effects contribution to the definition of the maximum time step and also because of the stronger mesh size variations over the computational domain.

RESULTS

The numerical method previously described was applied to the computation of both steady and unsteady flow fields. The steady computations were performed to assess the basic code steady-flow prediction capability, and the method was applied to the computation of the flow within the low-turning fan rotor blade section shown in figure 5. The blade was designed by J. Sanz (Sanz, 1988, 1989) for an inlet Mach number of $M_1 = 0.20$ and an inlet flow angle of $\beta_1 = 70.00°$ (with reference to the axial direction). The blade provides low turning, giving an outlet flow angle of $\beta_2 = 65.00°$ and reducing the flow speed to an outlet Mach number of $M_2 = 0.16$. The pitch-to-chord ratio is 0.75, the maximum thickness-to chord ratio is 0.05, and the blade chord is about 0.10 m.

The steady-flow computation was performed as a transient computation, starting from initial no-flow conditions and suddenly decreasing the outflow static pressure to the prescribed steady value. The required consistency in time reduces the convergence properties with respect to those obtained in pseudo-unsteady methods (Boretti, 1989b), but the aim of this analysis is the simulation of an unsteady flow behavior, not better convergence to a steady state.

At the beginning of the calculations, the inflow and outflow boundary conditions are given as follows

$$p_{01} = 100\ 000\ N/m^2$$

$$\rho_{01} = 1.21\ kg/m^3$$

$$\beta_1 = 70.00°$$

$$Tu_1 = 0.05$$

$$Le_1 = 0.005 \text{ m}$$

$$p_2 = p_{01}$$

The outflow static pressure is then suddenly reduced to the steady value

$$p_2 = 98\ 000 \text{ N/m}^2$$

and the flow starts to exit from the computational domain. After a certain number of time steps, a new steady-flow condition is reached.

The unsteady flow was simulated on the NASA-Ames Cray Y-MP. The computations were performed by using time steps of the order of 10^{-4} sec, close to the time step limit with CFL equal to unity. The two-stage scheme was selected during the computations, thus reducing the total computational effort. The advance of the flow equations in a computational grid made up of about 2000 grid points performing 10 000 time steps requires about 300 sec CPU time when solving the Navier-Stokes equations and about 200 sec CPU time when solving the Euler equations. The memory required is less than 0.3 megawords.

First, an Euler solution was performed. The computation mesh adopted in the inviscid computations is presented in figure 6. The grid is a 25 by 75 H-grid, made up of 25 computational points in the pitchwise direction and 75 computational points in the axial direction, with 41 computational points between leading and trailing edges. Figure 7 shows the computed surface Mach number distributions. The predicted flow field is very close to that expected, with a large velocity peak close to the blade leading edge followed by a smooth flow deceleration on the suction side and an almost constant velocity distribution on the pressure side.

The flow deceleration on the blade suction side can be strong enough to produce an undesired flow separation. In order to check the flow behavior on the rear suction side, a more accurate Navier-Stokes solution has been performed. The computational mesh adopted in the viscous computations is presented in figure 8. The grid is a 35 by 85 H-grid, made up of 35 computational points in the pitchwise direction and 85 computational points in the axial direction, with 49 computational points between leading and trailing edges. Figure 9 shows the computed constant velocity lines. The velocity is zero at the blade surface. The predicted Navier-Stokes flow field clearly shows the growth of the boundary layer over the blade surfaces. The growth on the rear suction side is particularly strong, but the adopted computational grid is not fine enough to allow the computation of recirculating flows. Further Navier-Stokes computations with higher grid refinement close to the blade rear suction side seem to be necessary before the final acceptance of the blade shape.

It is to be noted that oscillations of very low amplitude continue indefinitely, because of the wave reflections from the boundaries of the computational domain, but the influence of these oscillations on the blade pressure distribution is negligible.

Finally, the numerical method was applied to the computation of the rotor flow perturbed by the presence of downstream bodies. The computations were

performed by starting from initial steady conditions and then superimposing to the steady value for the exit pressure a sinusoidal dependence of the form

$$p_2(t) = 98\ 000\ [1 + 0.001 \sin (0.001t)]\ N/m^2$$

where t is the time in sec.

The successive integration of the Euler equations yields (after a certain number of time steps) a periodic flow condition, where the rotor pressure field follows an almost sinusoidal oscillation. Figure 10 shows an example of rotor pressure fluctuations on the blade suction and pressure side at the 80-percent chord position.

The computed pressure fluctuations are quite close to those expected, perhaps very close to those specified at the outflow boundary. The method appears to be able to simulate sinusoidal pressure oscillations without introducing strong nonphysical dissipations. Obviously, a better test case is required to properly determine the prediction capability of the code. Such a comparison will be possible only when experimental data are available in enough detail.

CONCLUSIONS

This paper has presented a time-accurate numerical method that can properly describe the steady and unsteady fan rotor flow fields in the blade-to-blade plane. The numerical integration algorithm reduces the computational cost of an unsteady simulation involving high-frequency disturbances in both CPU time and memory requirements. During the computations performed on the NASA-Ames Cray Y-MP supercomputer, the advance of the flow equations in a computational grid made up of about 2000 grid points performing 10 000 time steps requires about 300 sec CPU time when solving the Navier-Stokes equations and about 200 sec CPU time when solving the Euler equations. The memory required is less than 0.3 megawords. Thanks to the low computational cost and the good accuracy obtained during the simulations, the method appears to be a useful device to modify blade shape for better steady, aerodynamic performances. The code also indicates some ways to improve the unsteady aerodynamic performance.

APPENDIX - SYMBOLS

AV	artificial viscosity coefficient
a	speed of sound
abs	absolute
C	constant
C_ε	kinematic energy constant
C_μ	eddy viscosity constant
CFL	Courant-Friedrich-Levy stability criteria
D	wall term
D	diffusion vector
d_{ij}	Kronecker delta
dr	mesh size
dt	time step
E	wall term
ε	kinetic energy dissipation rate
F	compressibility term
f	function
f	unknown vector
G	compressibility term
h	enthalpy
K	turbulence kinetic energy
Le	length scale
M	Mach number
P	turbulence kinetic energy production
Pr	Prandtl number
p	pressure
q	heat flux vector

R_t turbulence Reynolds number

Sc Schmidt number

T residual vector

Tu turbulence level

t time

u velocity component

V velocity

β flow angle

γ specific heat ratio

κ heat transfer coefficient

μ viscosity coefficient

ρ density

τ viscous stress tensor

Subscripts:

t turbulent

0 total

1 inlet

2 outlet

Superscripts:

m time level

2 second order

4 fourth order

ACKNOWLEDGMENTS

The author would like to express his indebtedness to NASA Lewis Research Center, Cleveland, Ohio, and in particular to Dr. L. Povinelli, for their support to the present research activity. The author would also like to acknowledge Dr. Jose Sanz for his support in the use of the NASA Ames Numerical Aerodynamic Simulation Program and for the definition of the geometry of the blade cascade tested.

REFERENCES

Boretti, A.A.: An Explicit Runge-Kutta Method for Turbulent Reacting Flow Calculations. NASA TM-101945, 1989.

Boretti, A.A.: Transonic Viscous Flow Calculations for a Turbine Cascade With a Two Equation Turbulence Model. NASA TM-101944, 1989.

Boretti, A.A.; and Martelli, F.G.: Accuracy and Efficiency of a Time Marching Approach for Combustor Modeling. Fluid Validation of Computational Fluid Dynamics, Vol. 2, AGARD-CP-437-VOL-2, AGARD, Neuilly-Sur-Seine, France, 1988.

Chima, R.V.; Turkel, E.; and Schaffer, S.: Comparison of Three Explicit Multigrid Methods for the Euler and Navier-Stokes Equations. AIAA Paper 87-0602, Jan. 1987 (NASA TM-88878).

Groeneweg, J.F.; and Rice, E.J.: Aircraft Turbofan Noise. J. Turbomachinery, vol. 109, no. 1, Jan. 1987, pp. 130-141.

Hirsch, C.; and Deconinck, H.: Description of Various Flow Models From Navier-Stokes to Potential Flow Models. Thermodynamics and Fluid Mechanics of Turbomachinery, Vol. 1, A.S. Ucer, P. Stow, and C. Hirsch, eds., Martinus Nijhoff Publishers, Boston, 1985, pp. 3-85.

Jameson, A., et al.: Numerical Solutions of the Euler Equations by Finite Volume Methods Using Runge-Kutta Time-Stepping Schemes. AIAA Paper 81-1259, 1981.

Jones, W.P.; and McGuirk, J.J.: Mathematical Modelling of Gas Turbine Combustion Chambers. Combustor Modelling, AGARD CP-275, AGARD, Neuilly-Sur-Seine, France, 1979.

O'Brien, W.F.; Ng, W.F.; and Richardson, S.M.: Calculation of Unsteady Fan Rotor Response Caused by Downstream Flow Distortions. J. Propulsion Power, vol. 1, no. 6, Nov.-Dec. 1985, pp. 464-469.

Sanz, J.M.: Automated Design of Controlled Diffusion Blades. J. Turbomachinery, vol. 110, no. 4, Oct. 1988, pp. 540-544.

Sanz, J.M.: A Compendium of Controlled Diffusion Blades Generated by an Automated Inverse Design Procedure. NASA TM-101968, 1989.

Schmidt, W.; and Jameson, A.: Recent Developments in Finite-Volume Time-Dependent Techniques for Two and Three Dimensional Transonic Flows. Computational Fluid Dynamics, VKI-LS-1982-04, Von Karman Institute for Fluid Dynamics, Rhode-Saint-Genese, Belgium, 1982.

Scott, J.N.; and Hoo, E.A.: A Numerical Investigation of the Influence of Heating on the Excitation of High and Low Mach Number Jet Flows. J. Vibration, Acoustics, Stress Reliability Design, vol. 110, no. 1, Jan. 1988, pp. 104-111.

Sieverding, C.: The Base Pressure Problem in Transonic Turbine Cascades. Transonic Flows in Axial Turbomachinery, Vol. 2, VKI-LS-84-VOL-2, Von Karman Institute for Fluid Dynamics, Rhode-Saint-Genese, Belgium, 1976.

Smith, L.H., Jr.: Unducted Fan Aerodynamic Design. J. Turbomachinery, vol. 109, no. 3, July 1987, pp. 313-324.

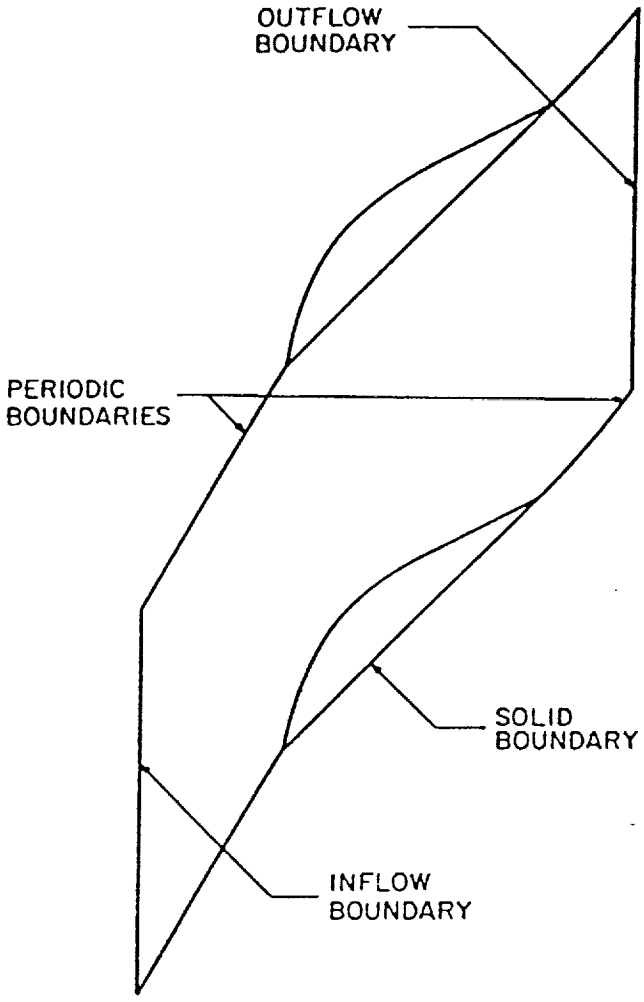

FIGURE 1. - FLOW DOMAIN.

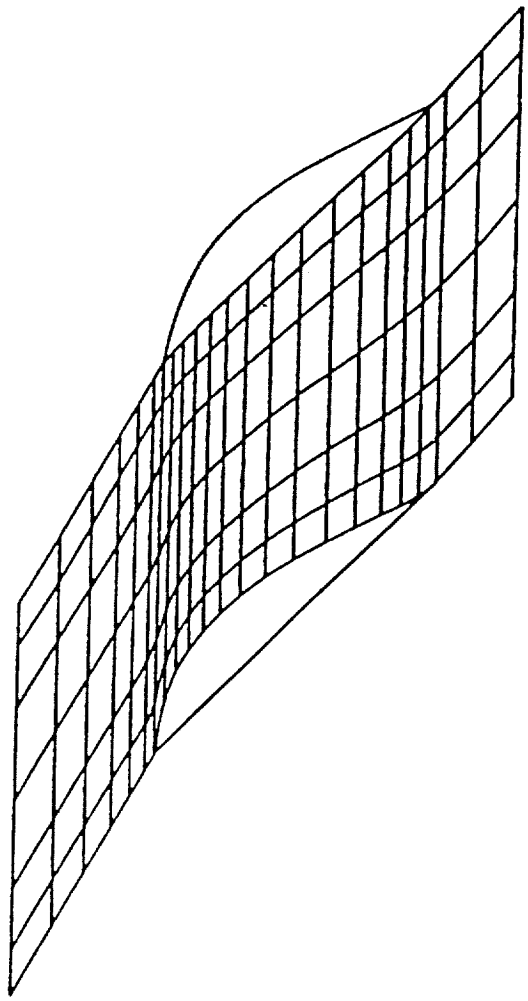

FIGURE 2. - COMPUTATIONAL DOMAIN.

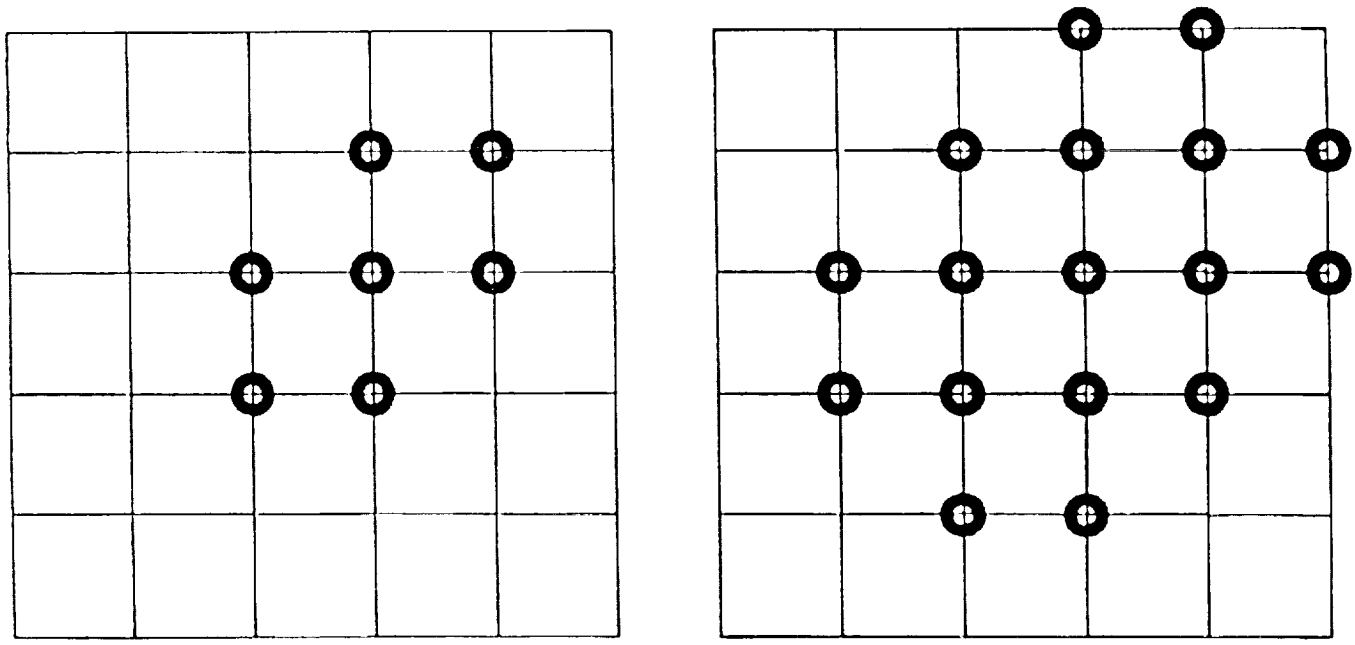

FIGURE 3. - INVISCID AND VISCOUS TERMS FINITE-VOLUME APPROXIMATION.

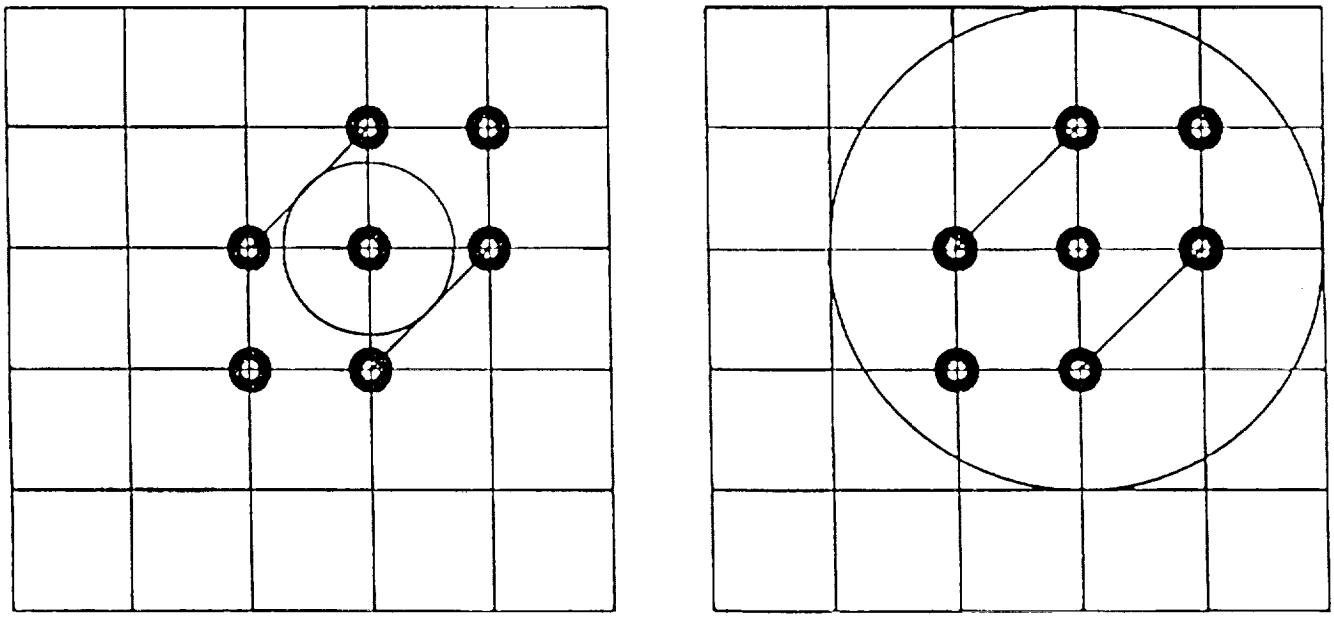

FIGURE 4. - STABLE TIME STEPS AT DIFFERENT COURANT-FRIEDRICH-LEVY STABILITY CRITERION (CFL) NUMBERS.

Inlet Mach No. 0.200	*Exit Mach No.* 0.163
Inlet Air Angle 70.00	*Exit Air Angle* 64.99
Turning 5.01	*Solidity* 1.332

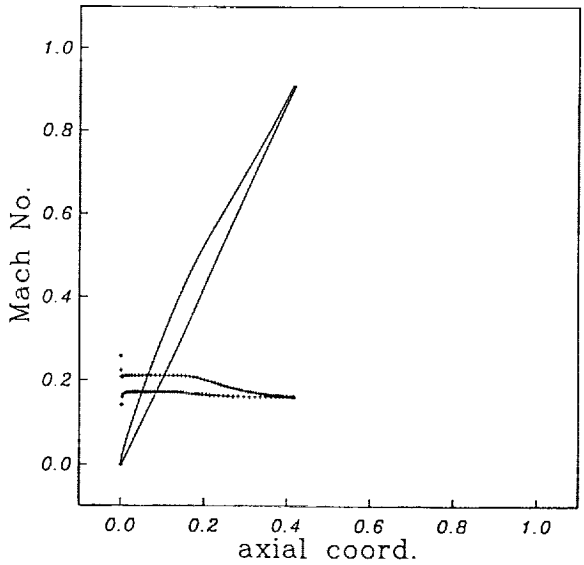

Max Thick 0.046	*Cap/chord* 0.751
T.E. Thick 0.005	*D.T.E* 0.000

FIGURE 5. - BLADE CASCADE TESTED.

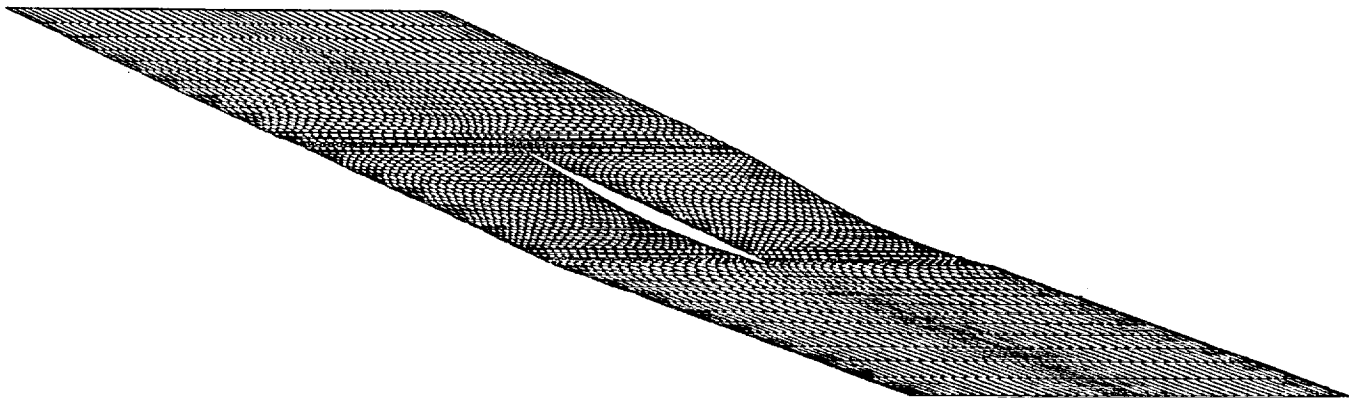

FIGURE 6. - EULER COMPUTATIONAL GRID.

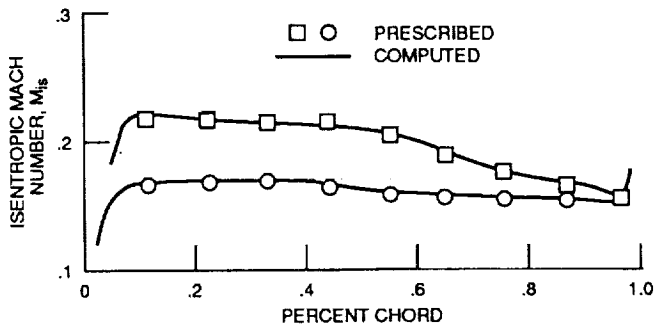

FIGURE 7. - COMPARISON OF PRESCRIBED AND COMPUTED SURFACE MACH NUMBER DISTRIBUTIONS.

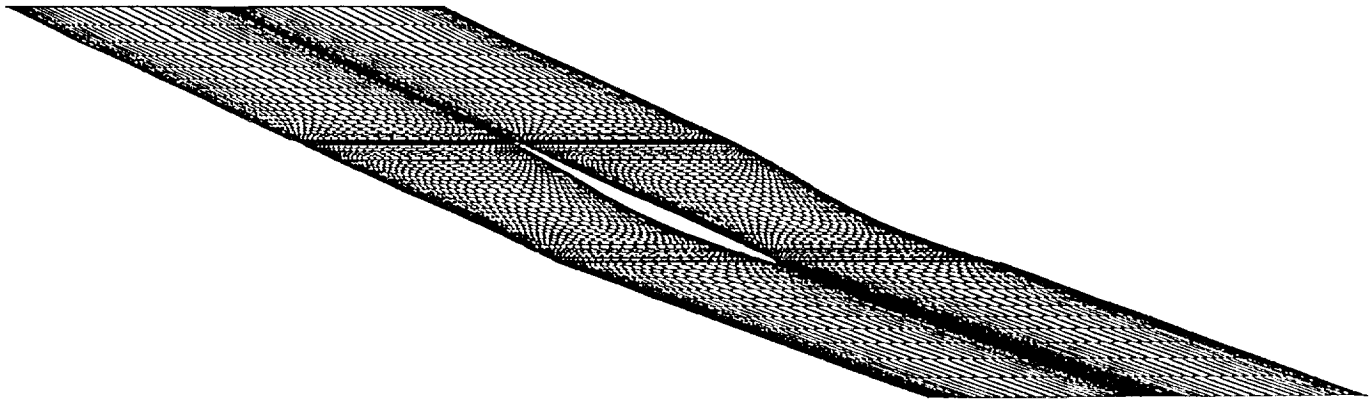

FIGURE 8. - NAVIER-STOKES COMPUTATIONAL GRID.

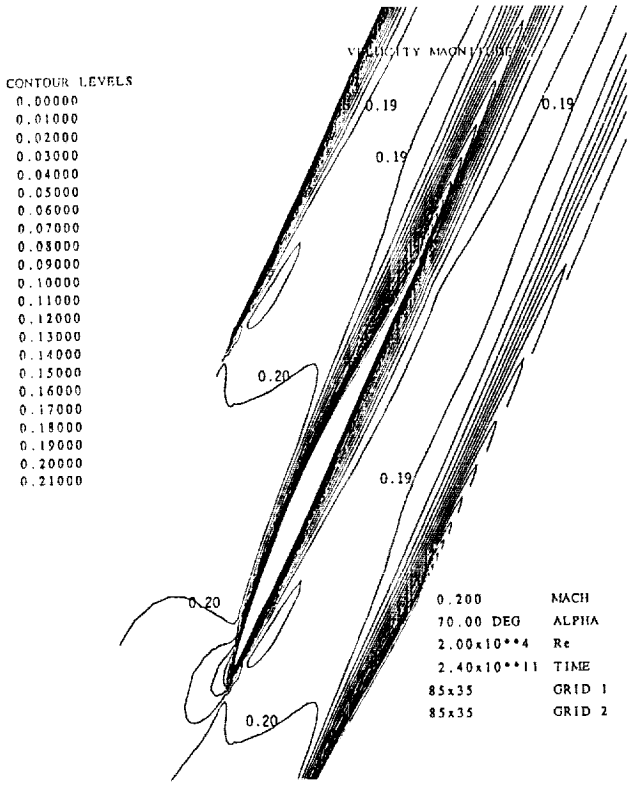

FIGURE 9. - COMPUTED MACH NUMBER CONTOURS.

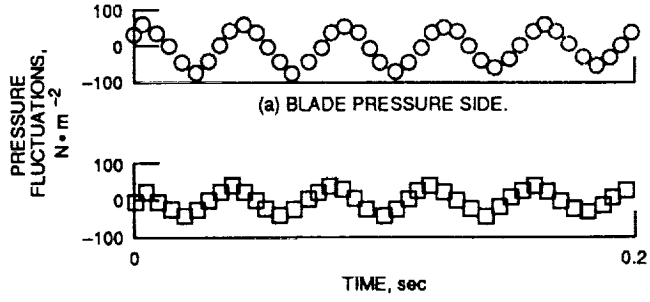

FIGURE 10. - PREDICTED ROTOR PRESSURE FLUCTUATIONS.

NASA
National Aeronautics and Space Administration

Report Documentation Page

1. Report No.	2. Government Accession No.	3. Recipient's Catalog No.
NASA TM-102402 ICOMP-89-29		

4. Title and Subtitle	5. Report Date
Two-Dimensional Euler and Navier Stokes Time Accurate Simulations of Fan Rotor Flows	July 1990
	6. Performing Organization Code

7. Author(s)	8. Performing Organization Report No.
A.A. Boretti	E-5155
	10. Work Unit No.
	505-62-21

9. Performing Organization Name and Address	11. Contract or Grant No.
National Aeronautics and Space Administration Lewis Research Center Cleveland, Ohio 44135-3191	
	13. Type of Report and Period Covered
	Technical Memorandum

12. Sponsoring Agency Name and Address	14. Sponsoring Agency Code
National Aeronautics and Space Administration Washington, D.C. 20546-0001	

15. Supplementary Notes

A.A. Boretti, Sistemi Elettronici Tecniche di Controllo, Centro Ricerche FIAT—MOTORI, Orbassano, Italy, and Institute for Computational Mechanics in Propulsion, Lewis Research Center, Cleveland, Ohio (work funded by Space Act Agreement C-99066-G). Space Act Monitor, Louis A. Povinelli.

16. Abstract

This report presents two numerical methods to describe the unsteady flow field in the blade-to-blade plane of an axial fan rotor. These methods solve the compressible, time-dependent, Euler and the compressible, turbulent, time-dependent, Navier-Stokes conservation equations for mass, momentum, and energy. The Navier-Stokes equations are written in Favre-averaged form and are closed with an approximate two-equation turbulence model with low Reynolds number and compressibility effects included. The unsteady aerodynamic component is obtained by superposing inflow or outflow unsteadiness to the steady conditions through time-dependent boundary conditions. The integration in space is performed by using a finite-volume scheme, and the integration in time is performed by using k-stage Runge-Kutta schemes, k = 2,5. The numerical integration algorithm allows the reduction of the computational cost of an unsteady simulation involving high-frequency disturbances in both CPU time and memory requirements. Less than 200 sec of CPU time are required to advance the Euler equations in a computational grid made up of about 2000 grid points during 10,000 time steps on a CRAY Y-MP computer, with a required memory of less than 0.3 megawords.

17. Key Words (Suggested by Author(s))	18. Distribution Statement
Euler equations Internal flows Runge Kutta	Unclassified – Unlimited Subject Category 02

19. Security Classif. (of this report)	20. Security Classif. (of this page)	21. No of pages	22. Price*
Unclassified	Unclassified	22	A03

NASA FORM 1626 OCT 86

*For sale by the National Technical Information Service, Springfield, Virginia 22161